Journal of Advanced Engineering Trends
ISSN : 2682 - 2091

Vol. 44, No. 2, July 2025

Hybrid Cooling System of an IPMSM for Electric Vehicle Traction Applications

Emad G. Shehata[1,*], Gamal R. H. Abo Elyamin[2]

[1] *Electrical Engineering Dept., Faculty of Engineering, Minia University, Minia, Egypt*
[2] *Dept. of Mechanical Power and Energy Engineering, Faculty of Engineering, Minia University, Minia, Egypt*
** Corresponding author(s) E-mail: emadgameil@mu.edu.eg*

ARTICLE INFO

Article history:
Received:30 May 2025
Accepted: 23 July 2025
Online: 23 July 2025

Keywords:
Electric Vehicles
IPMSM
Electromagnetic analysis
Hybrid cooling system
Thermal Analysis

ABSTRACT

An improved hybrid ventilation method of interior permanent magnet synchronous motor (IPMSM) is proposed to improve its thermal and electrical characteristics. Increasing motor temperature affects the stator winding and the permanent magnet (PM) inserted in the rotor. The water jacket method was proposed in different traction systems; however, the total weight and cost were increased. To increase the effectiveness of the cooling system, stator and rotor ducts are inserted to increase heat exchange between inner parts and external cooling water. One-layer ducts are inserted into the stator and two-layer ducts are inserted into the rotor. However, the ducts may affect the flux density in the rotor and stator which increases saturation level and degrades the electromagnetic performance. Optimum design is performed to determine the size of the stator and the rotor ducts. The effect of the designed ducts on electromagnetic and thermal performance is analyzed using two-dimensional finite element method. The performance of the proposed method is evaluated under short transient and standard duty cycle operation. The numerical results show effective reduction in stator winding and PM temperature. Under short peak power transient, the maximum temperature of the PM decreases from 78 to 60 ºC and the maximum temperature of the stator winding decreased from 177 to 167.9 ºC. During long transient, the temperature of PM and stator winding are 85 ºC and 101 ºC, respectively.

1. Introduction

Increasing energy needs and global warming concerns have ushered in the development of electric vehicle (EV) technology [1]. The global demand for EVs is increasing with time because EVs are considered as one of the main solutions of energy and climate problems. Many traction systems of pure and hybrid electric vehicles are propelled by permanent-magnet synchronous motors (PMSMs) [2-8]. The features of PMSM, such as high-power density, torque density, high efficiency, low noise, and maintenance-free operation, make it an ideal choice for EV applications. However, PMSMs still suffer from some drawbacks as follows:

i. The mechanical integrity of the rotor, especially the surface-mounted permanent magnets (PMs) type, has a problem for high-speed operation. Using interior permanent magnet synchronous machines (IPMSMs) overcome the problem of high speed where the PMs are inserted inside the rotor core [2-4].
ii. Because of the inherently uncontrollable PM flux, the constant-power operating range is limited. Using highly advanced control algorithms such as vector control and direct power/torque control extended the constant power range to acceptable range [4-8].
iii. In case the machine is not properly designed or operated, the PMs may be accidentally demagnetized by high armature reaction field or under high operating temperatures [9- 12].

Different solutions have been studied to improve the IPMSM performance and avoid the effect of temperature and demagnetization problem. In [9], the effects of PM dimension on the demagnetization characteristic are investigated. Analytical method is proposed to obtain minimum PM volume taking the machine anti-demagnetization ability into consideration. In [10], PM demagnetization characteristic is analyzed considering the recoil line to establish a base capable of securing the reliability of IPMSM for traction. In [11], to overcome PM demagnetization, a V-type combined pole IPMSM is proposed. Influences of magnetic-pole geometry on electromagnetic performance are investigated. To reduce the risk of PM demagnetization during assembly, a magnetizing device to magnetize V-type rotors is designed. The thermal circuit of the PMSM is established and the demagnetization characteristics of the machine at different temperatures are analyzed [12].

High cooling capacity liquid cooling is used by means of liquid circulation in a cylindrical water jacket [13]. The heat generated from the electric motor must be absorbed by the coolant circulating in the water jacket and moved to the radiator. A mixture of ethylene glycol and water of ratio 50-50 is proposed

to be used as a cooling liquid to dissipate about 5500 W of heat at temperature difference of 15 ºC between the inlet and outlet of coolant at constant mass flow rate. The resistance of copper wire increases as temperature increases and the permanent magnet can lose its magnetism, and the power loss is significantly affected by high temperature. The proposed model in [14] mentioned that the maximum temperature in the 35 kW motor was 120 ºC at the stator winding but it is intrinsic to maintain the outlet temperature of cooling water for motor and its drives below 60 ºC applying coolant flow rate of 11.2 *l/min* by a water pump. An evaluation of electromagnetic and thermal performance for traction motor that used in electric vehicles has been conducted in [15]. To perform the analysis, two different driving cycles are applied to urban and highway driving conditions by using three different motors. The thermal analysis evaluates the working conditions of the magnet and the windings for the motors and represents the effect of temperature on the performance then provides suggestions for traction motor design. It is concluded that forced cooling is required to enhance the motor performance by cooling down the winding temperature. As a modification of an IPM motor, a finned housing without forced cooling and with water cooling have been applied to improve the traction motor performance in [16]. Using conductors with high thermal conductivity insulation can reduce temperature and the cooling process has been enhanced by applying forced cooling with the suitable flow rate to reduce winding temperature. The magnetic losses and heat generation give an indication of the performance and the life expectancy of the traction motor [17]. Extremely high temperatures rapidly damage the insulation and reduce the function of some essential components such as winding conductors and demagnetize the motor permanent magnet. Hence, reducing the temperature of the rotor may boost motor efficiency. To achieve the cooling process, thermal design is carefully considered for both passive and active cooling methods.

In this paper, a new hybrid cooling method is proposed for cooling of V-type IPMSM machine. The main cooling method is using an external water jacket cooling system. To improve the cooling process, ventilation ducts are inserted into the stator and rotor cores. One layer of ventilation ducts is inserted in the stator and two layers of ventilation ducts are inserted in the rotor. The main function of the ducts is improving heat exchange between inner parts and external parts. Determination of the ducts place and cross section area is important to avoid core magnetic saturation. However, the duct area can increase core magnetic saturation which increases motor temperature and degrades performance. The cross-section area of the ducts is optimized to improve cooling and avoid magnetic saturation. The electromagnetic and thermal performance is analyzed under different operating conditions using 2-D finite element method.

2. IPMSM design

Cross-section view of the proposed IMPSM is shown in Figure 1a. The motor has two layers of PMs inserted in the rotor core. The inner layer is V-type PM while outer layer is tangential type. The stator winding is a conventional three phase winding. Outer water jacket cooling system was proposed. In this paper, the stator and rotor ducts are inserted as shown in Figure 1b. The dimensions of the proposed IPMSM are given in Table 1.

The stator and rotor cores are made of silicon steel M250-35A. The PMs are made of Sintered Neodymium-Iron-Boron Magnets (N42UH). The stator winding is made of annealed copper. The thermal conductivity, specific heat and density of the different materials are given in Table 2. For stator winding, temperature coefficient of resistivity of copper = 0.00393 and its resistivity 1.724e-8 at 20 ºC.

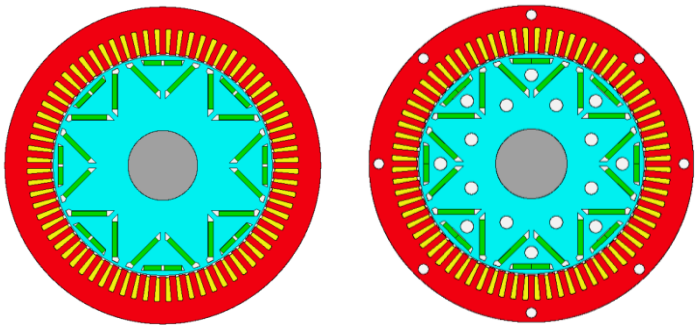

a. IPMSM without ducts b. IPMSM with ventilation ducts.

Figure 1: Cross-section view of old and proposed topologies

Table 1: IPMSM dimensions

Parameters	Value	Parameters	Value	Parameters	Value
Stator outer Dia.	250 mm	Stack length	100 mm	Tooth width	4.5 mm
Stator bore	175 mm	Air gap length	0.8	Slot depth	19 mm
No. Of solts	72	Rotor type	Interior V + Tangential	Slot corner Raduis	1 mm
No. Of poles	8	Shaft Dia [F]	45 mm	Tooth Tip depth	1 mm
Shaft Dia.	55	Shaft Dia [R]	45 mm	Slot opening	3 mm
Motor length	240 mm	Slot type	Parallel	Tooth Tip angle	40 Deg.

Table 2: Thermal characteristics of motor materials

Component	Material	Thermal conductivity W/M/C	Specific Heat kJ/kg/ºC	Density kg/m^3
Stator/Rotor lamination	M250-35A	30	0.46	7650
Stator winding	Copper (Annealed)	401	0.385	8933
Magnet	N42UH	7.6	0.46	7500

3. Motor loss

The losses in the IPMSM are the source of heat. There are copper loss, magnet loss, iron loss, and mechanical loss. The relationship between input power (P_{in}), output power (P_{out}) and power loss (P_{loss}) are expressed as:

$$P_{in} = P_{out} + P_{loss} \quad (1)$$

$$P_{loss} = P_c + P_{pm} + P_{iron} + P_{mech} \quad (2)$$

where, P_c is the copper loss, P_{pm} is the permanent magnet loss, P_{iron} is the iron loss in cores of stator and rotor, and P_{mech} is the mechanical loss includes friction and windage losses.

3.1. Copper loss

Due to copper resistivity, an amount of power is lost in the winding when current flowing in it. The power loss raises the winding temperature which in turn increases winding resistivity. At high frequencies or high speeds, the resistance increases because of a skin effect phenomenon. The copper loss in three phase IPMSM can be expressed as:

$$P_c = 3i_{ph}^2 R_{ph} \quad (3)$$

The variation of stator resistance with temperature is based on temperature coefficient of copper:

$$R_{ph} = R_{ref}\left(1 + \alpha(T - T_{ref})\right) \quad (4)$$

Where, i_{ph} is the root-mean-square value of phase current, and R_{ph} is the phase winding resistance, R_{ref} is the phase winding resistance at 20 °C; α is the temperature coefficient of copper (which is 0.004/°C); and *T* is the winding temperature. The temperature of the stator winding under drive cycle reaches 160 °C.

The estimated stator resistance of the proposed IPMSM at 100 °C = 0.008557 Ohms/Phase.

At peak power, the phase current = 560 Arms.

The copper loss= 3*5602*0.008557 = 8.05 kW.

3.2. PM loss

The loss in the PM is mainly due to the time-varying magnetic field. The known two terms of magnet loss are hysteresis and eddy current losses. Both types depend on the operating point of the PM, operating frequency and air gap flux density. Because of the non-sinusoidal stator current (time harmonics) and nonuniform air gap flux (space harmonics), the air gap magnetic field has fundamental and harmonic components which increase magnet and core loss.

The magnet loss is usually calculated by [19]

$$P_{pm} = \frac{\sigma}{24} L_{pm} T_{pm} W_{pm}^3 B^2 F^2 \quad (5)$$

Where L_{pm}, T_{pm}, Wpm are the PM length, thickness and width, respectively. σ is the electric conductivity of the magnet material, *B* is the air gap flux density, and *F* is the harmonic component frequency. Figure 2 shows the waveform of the sinusoidal flux density. It is shown that the waveform has different harmonic components which increase PM loss.

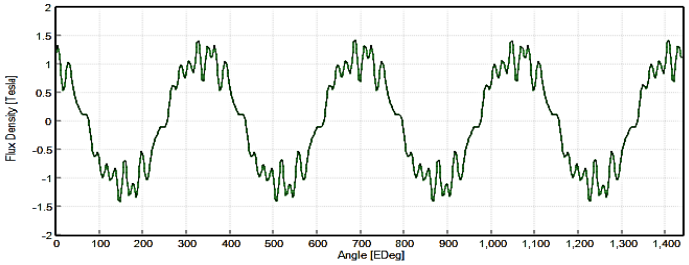

Figure 2: Air gap flux density at loading (peak power)

At high-speed operation and high frequency, eddy current loss is the main loss in PMs. The higher-order time harmonics of the current waveform is basically generated by the inverter. The rare-earth neodymium (NdFeB) magnet, which is used in the proposed IPMSM, its Curie temperature is 330 °C, above which the magnet is totally demagnetized. However, the magnet temperature is not allowed to rise higher than 100 °C to prevent irreversible demagnetization when the coercivity and remanence of the magnet deteriorate during the EV operation.

B-H curve of PM material (N42UH) at different operating temperature degrees is given in Figure 3. At 100 °C, residual flux density B_r=1.2 T and H_c = 0.9*10^6 A/m and polarization J=1.18. The non-linear demagnetization characteristics for magnets used can be expressed as [18]

$$B_t = B_r + \mu_0 \mu_r H - E.e^{-k_1(k_2+H)} \quad (6)$$

where B_t is the total flux density of the magnet, B_r is the magnet's residual induction (which is calculated at the appropriate temperature using α), μ_0 is the permeability of free space. μ_r is the magnet's relative permeability = 1.05, H is the demagnetizing field strength, E is a dimensional conversion factor E = 1 T, and k_1 is the Squareness Factor = 6e-5 , k_2 is a constant defined by [18]:

$$k_2 = -\left[\left(B_r + (\mu_r - 1)\mu_r H_{cJ}\right)\frac{1}{E}\right]/k_1 - H_{cJ} \quad (7)$$

where H_{cJ} is the magnet's intrinsic coercivity (which is calculated at the appropriate temperature)

The temperature dependence of B_r and H_{cJ} is encoded through the relations [18]:

$$B_{r\,Mag\,temp} = B_{r\,Tref}\left(1 + \frac{\alpha.(T_{mag\,temp} - T_{mref})}{100}\right) \quad (8)$$

$$H_{cJ\ Mag\ temp} = H_{cJ\ Tref}\left(1 + \frac{\beta.(T_{magtemp} - T_{mref})}{100}\right) \quad (9)$$

The reversible temperature coefficients (RTCs) can be estimated as follows:

$$\alpha = \frac{(B_{r\,Tref} - B_{r\,Mag\,temp})}{B_{r\,Tref}\,(T_{mag\,temp} - T_{mref})} \quad (10)$$

$$\beta = \frac{\left(H_{cJ_{Tref}} - H_{cJ\,Mag\,Temp}\right)}{H_{cJ_{Tref}}(T_{mag\,temp} - T_{mref})} \quad (11)$$

where, B_{rTref} is the residual induction (at the reference temperature T_{ref} = 20 ºC) = 1.31 as shown in figure 3. H_{cJ} is the intrinsic coercivity at the reference temperature = 1.99e6, the reversible temperature coefficients α = - 0.12 and β = - 0.46.

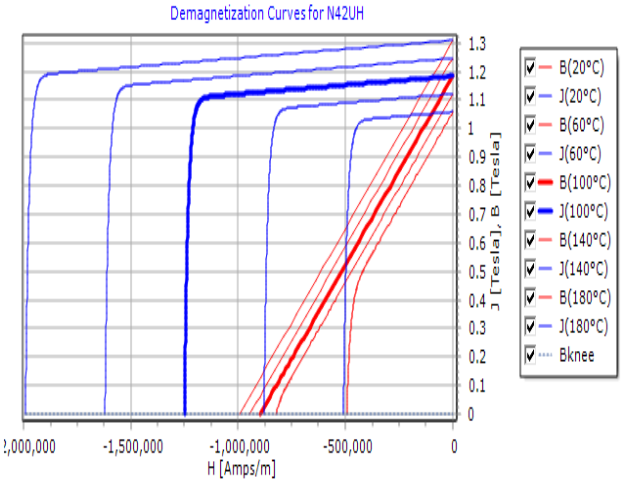

Figure 3: Demagnetization curves of PM material N42UH at different temperature degrees [11]

3.3. Core loss

Time varying magnetic field generates power loss in the motor core. The main two terms of core loss are hysteresis loss and eddy current loss. In turn, core loss is proportional to motor speed or frequency. The two terms of core losses can be estimated as:

$$P_c = P_h + P_e = k_h f B_{max}^n + k_e f^2 B_{max}^2 \quad (12)$$

Where, k_h and k_e are the material-dependent coefficients of hysteresis loss and eddy current loss, which depends on magnetic core characteristics and core lamination thickness. B_{max} is the maximum air flux density, and n is a material-dependent exponent between 1.5 and 2.5.

The manufacturer's data sheet usually provides core loss curves, which allow estimation of the material-dependent coefficients in the core loss polynomial as a function of flux density and frequency. Here, only the fundamental sinusoidal current was considered. Figure 4 shows the data sheet of the proposed core material (M250-35A). For the same motor speed, the core loss decreases as temperature rises. This is due to the demagnetization effect of the magnet when the temperature rises.

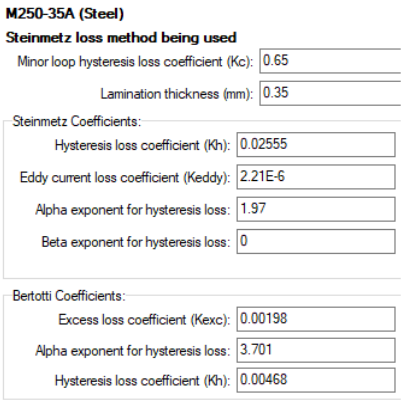

Figure 4: Data sheet of silicon steel M250-35A [11]

3.4. Mechanical loss

Mechanical losses are a consequence of bearing friction losses, windage losses of rotating rotor, and ventilator losses. Bearing losses depend on the shaft speed, type of bearing, lubricant properties and the load on the bearing. Bearing manufacturers give guidelines for calculating bearing losses. Bearing friction losses are [19]:

$$P_b = 0.5\Omega\mu F_b D \quad (13)$$

Where, Ω is the angular frequency of the shaft supported by a bearing, μ the friction coefficient (typically 0.08 – 0.20 for steel-on-steel sliding contact surface combination), F_b the bearing load and D is the inner diameter of the bearing.

Windage losses are due to the friction between moving parts and surrounding air so depends on rotor speed. The windage losses are; the losses in the air gap and the losses at the ends of the rotor. The air-gap part of the rotor can be modeled as a rotating cylinder in an enclosure. Gives an equation for the power associated with the resisting drag torque of the rotating cylinder.

$$P_{\rho w} = \frac{1}{32} k C_M \pi \rho \Omega^3 D_r^4 l_r \quad (14)$$

where, k is a roughness coefficient (usually k = 1–1.4, for a smooth surface k = 1,), C_M the torque coefficient, ρ is the air density, Ω is the rotor angular velocity, D_r the rotor diameter, and l_r the rotor length.

4. Proposed cooling method of IPMSM

Since the IPMSM performance can be limited by the thermal conditions, water cooling is proposed to reduce the winding and magnet temperature under working conditions to fulfill the requirements of the driving cycles for IPMSM. In the current study, a modified design of IPMSM has been conducted. One-layer ducts are inserted in the stator and two-layer ducts are inserted in the rotor as shown in Figure 1b. See Table 1 for

dimensions of the proposed IPMSM. Figure 5 shows the two types of ventilation.

Electric motors are cooled by air ventilation due to the low heat generation compared to the traditional internal combustion engine. If the required cooling capacity in large motors is high, then liquid circulation cooling is applied. Liquid cooling can also be used in small motors to enhance the overall cooling process. Liquid cooling system has higher cooling efficiency, greater power/size ratio, and lower noise level if compared to air cooling. The generated heat from the electric motor is collected by the coolant circulating in the water jacket. The coolant was assumed to be ethylene glycol and water mixture at 50-50 ratio (EGW 50/50).

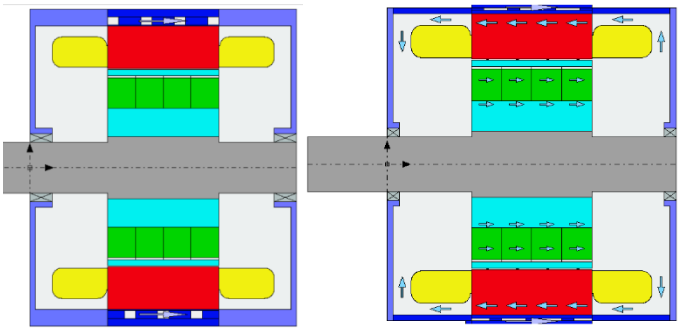

a. Standard air ventilation b. Hybrid air ventilation and EGW cooling

Figure 5: Air ventilation 'without cooling ducts' and air ventilation 'with EGW cooling ducts'

4.1. IPMSM heat transfer analysis

The IPMSM runs at peak power condition of 200 kW. If the motor without forced cooling has an efficiency of 90 % then, 10 % of the power loss can be assumed as heat generated by the motor which equal to 20 kW. The cooling system is assumed to dissipate about 24.4 kW as 1.22 safety factor is used. The rate of heat transfer is given by:

$$\dot{Q}_{gen} = \dot{m} c_p \Delta T_{max} \quad (15)$$

where, $\dot{m}$ is the mass flow rate, c_p is the specific heat of the coolant and ΔT_{max} is the maximum temperature difference between coolant and electric motor space.

By applying air ventilation in the standard motor, in this case air is used as a coolant and the heat load has to be removed by the cooling process according to (15). If the temperature difference is limited to 15 ºC [13] and the c_p for air is 1.009 kJ/kg.K as shown in Table 3, then a constant mass flow rate of 1.614 m^3/s has to be maintained to remove the 24.4 kW of the generated heat which is very difficult to achieve so a modified design applying hybrid air ventilation and EGW cooling system is proposed.

For the proposed water cooling arrangement, as taken from Table 3, where the coolant inlet temperature is 65 ºC, and the maximum winding temperature is 95.5 ºC, then ΔT_{max} is 30.5 ºC. Fluid volume flow rate is 8 l/min., density of the EGW coolant is 1051 kg/m^3, specific heat of the EGW coolant is 3.504 kJ/kg.K and coolant velocity are 2.672 m/s.

Table 3: Thermal characteristics of air and liquid coolant EGW

	Air	EGW 50/50
Thermal conductivity	0.03027	0.411
Density (kg/m^3)	0.998	1051
C_p (kJ/kg.K)	1.009	3.504
Kinematic viscosity	2.09e-5	1.305 E-6
Dynamic viscosity	2.088e-5	0.00137
Fluid volume flow rate (l/min)		8

Based on the aforementioned data, the heat load that coolant can dissipate is calculated using (15) as 14.976 kW. So the proposed cooling system can dissipate 14.976 kW deducted from 24.4 kW and the remaining heat loss that affects the efficiency is 9.424 kW. Hence, the calculated efficiency is 95.288% here, only the loss due to heat generation is considered. Any additional losses will definitely reduce the efficiency of the system. Referring to the system efficiency illustrated in Table 4 and the calculated efficiency, the difference between the calculated efficiency and the tabulated one is a result of considering the other losses in the system.

5. Results and discussion

In the following sections, the electromagnetic and thermal performance of the proposed IPMSM with hybrid ventilation method will be analyzed under different operating conditions.

5.1. Electromagnetic performance analysis

Electromagnetic analysis is carried out under peak power on conventional IPMSM. Figure 6 shows the air gap magnetic flux density and flux lines in different parts of the motor under peak power conditions (200 kW). The results are used to select the optimum place of rotor ducts. It is shown that there is a dead area in the rotor core (black circles), so circular ducts could be inserted in the rotor to improve motor ventilation without affecting the flux density. Figure 7 shows the flux paths in rotor and the location of the stator and rotor ducts. The outer layer of rotor ducts is inserted in the center between each pole parts while in the inner layer is inserted between each two poles. The arbitrary ducts diameters are; stator duct diameter of 6 mm and rotor duct diameter of 10 mm. Figure 8 shows the flux density and flux lines in different parts. It is shown that there is no change in rotor circuit. But compared to Figure 6, saturation appears in the stator core because of stator ducts. So, stator duct diameter needs optimum design.

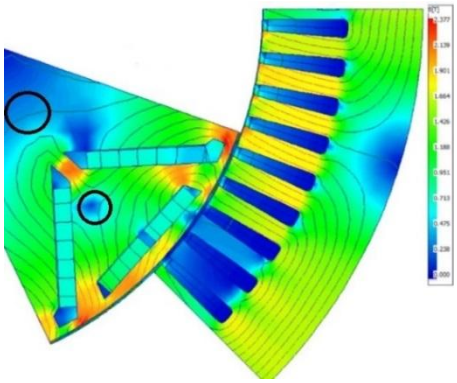

Figure 6: Flux density and flux lines under peak power conditions

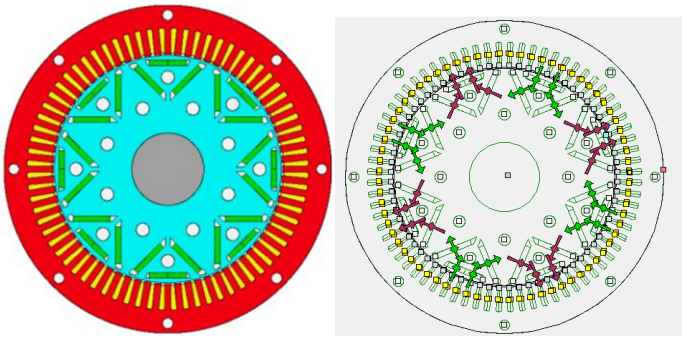

Figure 7: Stator and rotor ducts for ventilation

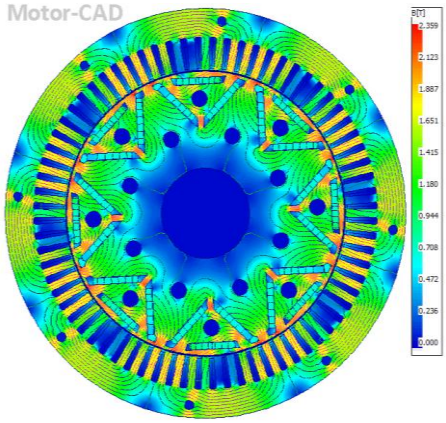

Figure 8: Flux density and flux lines under peak power loading

To study the effect of stator duct area on electromagnetic performance, sensitivity analysis is carried out. The stator duct diameter is changed from 0 to 10 mm. Figure 9 shows the variation of motor torque, line to line back EMF and efficiency. It is shown that stator duct diameter 6 mm has negligible effects of back EMF and motor torque. So, the following study will be carried out using 6 mm stator duct diameter.

Figure 9 and Figure 10 show the motor performance under peak power loading with 6 mm stator duct diameter. The results show that the motor preserves the Torque- speed and power-speed characteristics. The proposed IPMSM has suitable characteristics in the regions of constant torque and constant power. The motor could develop the maximum torque from standstill till 8000 rpm (constant torque region) and rated torque (150 N.m) till operating speed over 14000 rpm. The results illustrate that the proposed motor has a wide field weakening region. Efficiency-torque map in Figure 11 shows the motor operates in high efficiency for wide operating region.

Figure 9: Effect of stator duct diameter on peak torque, back Line-Line EMF rms, and efficiency

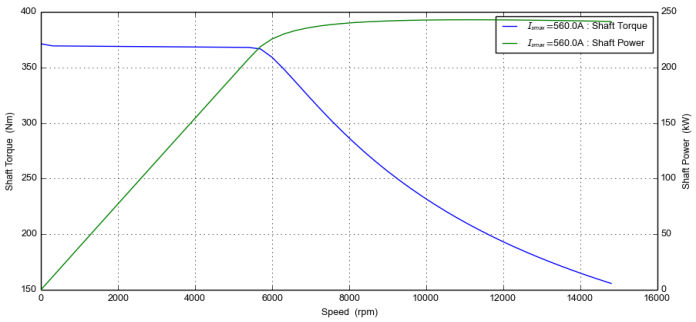

Figure 10: Torque -speed and power-speed curves of the proposed IPMSM

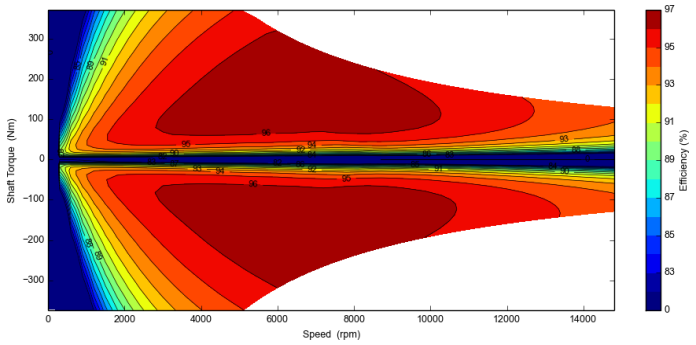

Figure 11: Shaft torque and efficiency map of the proposed IPMSM

The motor losses under peak power are given in Table 4. Most losses are in the stator winding and iron. Good ventilation of stator parts achieves high efficiency and long life of motor parts.

Table 4: Summarized losses in IPMSM under peak power loading

Input power	201.31kW	Stator copper loss	8.05 kW
Phase current	560 Arms	Magnet loss	0.02098 kW

Output power	191.41kW	Stator iron loss	1.484 kW
Shaft torque	365.56Nm	Rotor iron loss	0.04893 kW
Shaft speed	5000 rpm	Windage loss	0.01201 kW
System efficiency	95.08 %	Friction loss	0.1 kW
		Total losses	**9.904 kW**

5.2. Thermal performance analysis

The proposed cooling system keeps the parts of IPMSM maximum temperature less than that for the standard one. This modification enhances the motor performance by about 5% which keeps the motor working in its full or partial load for a longer period compared to the standard one without cooling. The performance of the motor under short and long transient can be illustrated as follows:

a. Short transient

The machine runs with peak load (375 N.m) and rated speed (5000 rpm) for 120 seconds. In this case, the machine is tested under short peak power transient. The temperature variation for stator, rotor, PM and winding are shown in Figure 12. It is shown that the winding temperature reached 154 ºC using the proposed design compared to 180 ºC without using ventilation ducts. The PM temperature reached 60 ºC compared to 72 ºC without using ventilation ducts. Figure 13 shows the temperature distribution in rotor and PM. It is shown that the maximum temperature is decreased from 78 to 60 ºC. Figure 14 shows the reduction in stator winding temperatures. The results show a significant reduction in temperature of different parts.

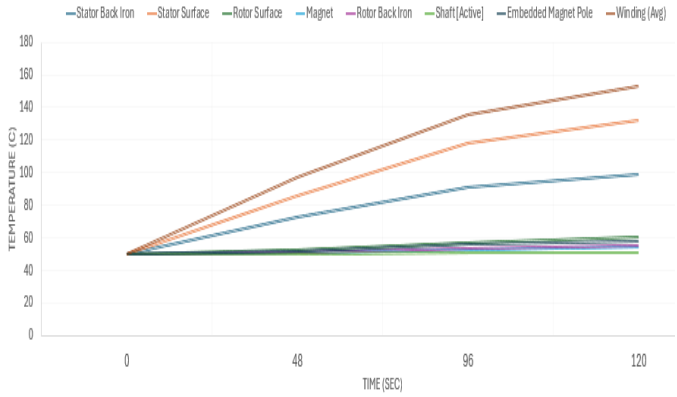

Figure 12: Temperature variation under peak power transient

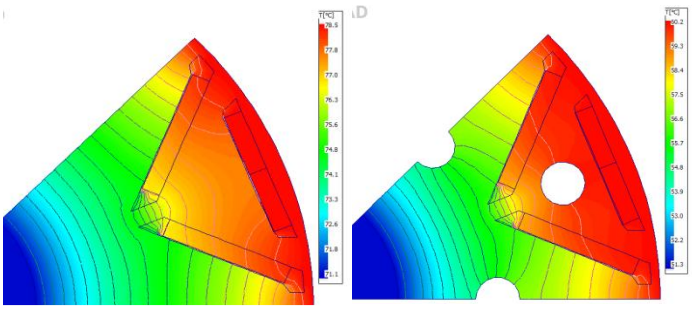

Figure 13: Temperature distribution in rotor under peak power short transient

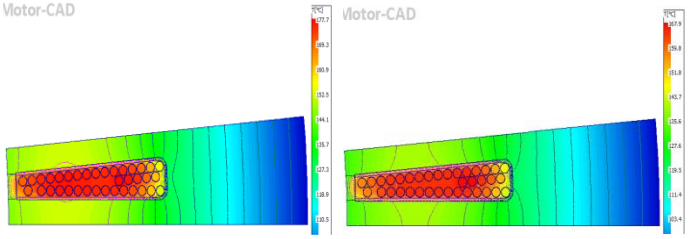

Figure 14: Temperature distribution in stator under peak power short transient

The effect of motor temperature on electromagnetic performance was re-evaluated taking thermal effect under full load into account. Thermal effects on torque-speed and power-speed characteristics are given in Figure 15.

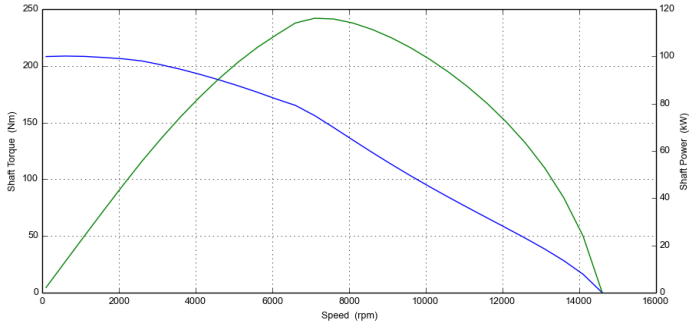

Figure 15: Torque-speed and power-speed characteristics taking thermal effect into account

The continuous torque requirement of 95 N.m is exceeded up to 10000 rpm. The continuous power requirement of 70 kW is available between 3000 rpm to 12000 rpm. The continuous power is close to the peak power. The machine is reaching the thermal limits just before maximum speed. Figure 16 illustrates the stator winding and PM temperature variation with motor speed. It is shown that winding temperature is reduced significantly at high speeds. At low speeds or low frequency, the copper loss is the main loss and core loss is less significant while at high speeds/frequencies, the core loss is the main loss.

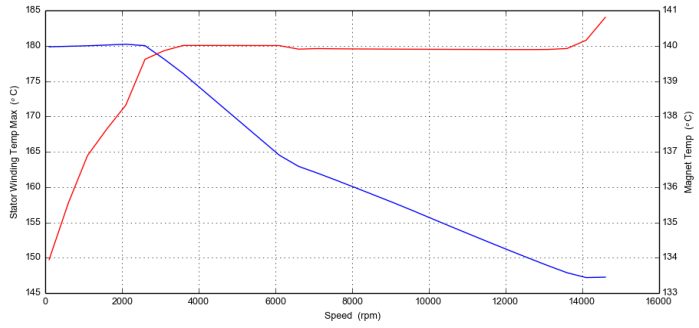

Figure 16: Stator winding and magnet temperature with speed under constant loading.

b. Long transient

In this case, the thermal performance will be evaluated under standard duty cycle drive WLTP3. The motor is tested for 5 drive cycles (9000 sec or 2.5 hours) where the drive cycle is 1800 sec (30 minutes). Figure 17 shows the torque and speed of the electric vehicle of the proposed drive cycle. Figure 18 shows the maximum stator winding temperature. It is shown that it is reduced from 94.1 to 91.4 ºC which indicates a significant cooling of stator winding.

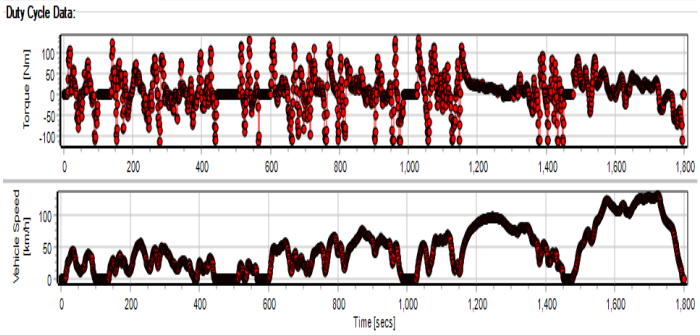

Figure 17: Standard drive cycle WLTP3 torque and speed

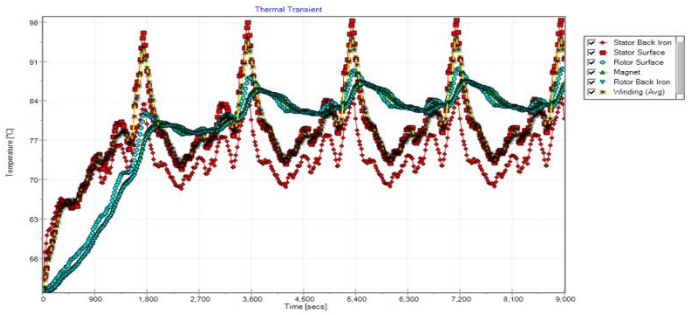

Figure 18: Temperature distribution in stator under peak power short transient

6. Conclusions

To improve thermal and in turn electromagnetic performance of IPMSM for electric vehicles traction, a hybrid ventilation method is proposed in this paper. The hybrid ventilation method consists of outer water jacket and inner air ducts in the stator and rotor cores. The main ventilation method is the outer water jacket, but inner air ducts improve ventilation of stator copper winding and inner permanent magnets. Different motor losses are calculated and in turn a cooling method is designed. Electromagnetic and thermal analysis is carried out with and without using air ducts. Two-Dimension finite element method was used for analysis.

The proposed hybrid method achieved the following benefits:

1. The weight of the motor is decreased because of air ducts in the stator and rotor cores.
2. The output power with the proposed hybrid ventilation method achieved the peak and rated power.
3. Under peak power during short transient, the maximum steady state temperature of the rotor and PM is decreased from 78.5 ºC (water jacket only) to 60.2 ºC (using a hybrid method).
4. Under peak power during short transient, the maximum steady state temperature of the stator copper winding decreased from 177.7 ºC (water jacket only) to167.9 ºC (using a hybrid method).
5. The rated continuous torque (95 N.m) is exceeded up to 10000 rpm. Continuous power (70 kW) is available between 3000 rpm to 12000 rpm.
6. For long operation, the maximum stator winding temperature is reduced from 94.1 to 91.4 ºC.

Conflict of Interest

The authors declare no conflict of interest.

References

[1] Mehrdad Ehsani , Krishna Veer Singh, Hari Om Bansal , and Ramin Tafazzoli Mehrjardi “State of the Art and Trends in Electric and Hybrid Electric Vehicles” Proceedings of the IEEE, Vol. 109, No. 6, June 2021, pp. 967- 984.

[2] Jung-Min Mun, Gyeong-Jae Park, SangHyeok Seo, Dae-Woo kim, Yong-Jae Kim, and Sang-Yong Jung “Design Characteristics of IPMSM with Wide Constant Power Speed Range for EV Traction” IEEE Trans. on Magnetics, Vol. 53, Iss.6, June 2017.

[3] Gilsu Choi 1, and Gerd Bramerdorfer “Comprehensive Design and Analysis of an Interior Permanent Magnet Synchronous Machine for Light-Duty Passenger EVs” IEEE Access, Vol. 10, 2022, pp. 819-831.

[4] Cheon-Ho Song, In-Soo Song, Hui-Seong Shin, Chung-Hui Lee, and Ki-Chan Kim “A Design of IPMSM for High-Power Electric Vehicles with Wide-Field-Weakening Control Region” IEEE Trans. on Magnetics, Volume: 58, Iss.2, February 2022.

[5] Zhuoran Huang, Zhidong Qin, Cheng Lin and Jilei Xing “A Parameter-independent Optimal Field-weakening Control Strategy of IPMSM for Electric Vehicles over Full Speed Range” IEEE Trans. on Power Electronics, Vol. 36, Iss.4, April 2021, pp. 4659 – 4671.

[6] Yue, Cao, Sean McLoone, and John Morrow “Design and Flux-Weakening Control of an Interior Permanent Magnet Synchronous Motor for Electric Vehicles” IEEE Transactions on Applied Superconductivity, Vol. 26, Iss.7, October 2016.

[7] Tae-Yong Lee, Myung-Ki Seo, Young-Yoon Ko, Yong-Jae Kim, Sang-Yong Jung “Electromagnetic Performances Analysis of IPMSM According to the Current Control Method Under Flux-Weakening Control Region” IEEE Trans. on Applied Superconductivity, Vol. 28, Iss.3, April 2018.

[8] Yongming Xu , Mengmeng Ai , Ziyi Xu , Wenhui Liu, and Yaodong Wang “Research On Interior Permanent Magnet Synchronous Motor Based on Performance Matching of Electric Bus” IEEE Transactions On Applied Superconductivity, Vol. 31, Iss.8, November 2021.

[9] Weinan Wang, Ping Zheng, Mingqiao Wang, Yong Liu, Zhenxing Fu, and Yi Sui “Demagnetization and Permanent-Magnet minimization Analyses of Less-Rare-Earth Interior Permanent-Magnet Synchronous Machines Used for Electric Vehicles” IEEE Trans. on Magnetics, Vol. 54, Iss.11, November 2018.

[10] Geochul Jeong, Hyunwoo Kim, and Ju Lee “A Study on the Design of IPMSM for Reliability of Demagnetization Characteristics-Based Rotor” IEEE Transactions on Applied Superconductivity, 2020, Vol. 30, Iss.4, June 2020s.

[11] Qingjian Wang, Hongfa Ding, Hang Zhang, Yiliang Lv, Haoran Guo, and Liang Li “Study of A Post-Assembly Magnetization Method of A V-Type

Rotor of Interior Permanent Magnet Synchronous Motor for Electric Vehicle" IEEE Transactions on Applied Superconductivity, Vol. 30, Iss.4, June 2020.

[12] Zhang Meiwei, Li Weili, and Tang Haoyue "Demagnetization Fault Diagnosis of the Permanent Magnet Motor for Electric Vehicles Based on Temperature Characteristic Quantity" IEEE Trans. on Transportation Electrification, Vol. 9, Iss.1, March 2023, pp. 759-770.

[13] Abdul Karim, Z.A. and A. Yusoff, "Cooling System for Electric Motor of an Electric Vehicle Propulsion" Advanced Materials Research, 2014. 903: p. 209-214.

[14] Chang, H.-Y.H., Y.-P. Yang, and F.K.-T. Lin "Thermal-fluid and electromagnetic coupling analysis and test of a traction motor for electric vehicles" Journal of the Chinese Institute of Engineers, 2018. 41(1): p. 51-60.

[15] Huynh, A. and M.-F. Hsieh "Performance Analysis of Permanent Magnet Motors for Electric Vehicles (EV) Traction Considering Driving Cycles" Energies, 2018. 11: p. 1385.

[16] Ki-O Kim;Young-Hoon Jung;Jin-Cheol Park;Myung-Seop Lim " Comparative study of Mechanical and Electrical Characteristics on High-Strength Steel and Conventional Steel for EV Traction High-Speed Multilayer IPMSM Using Rare-Earth Free PM" IEEE Transactions on Magnetics , 2023 | Vol. 59, Iss. 11: pp. 1- 5.

[17] Gai, Y., et al. "Cooling of Automotive Traction Motors: Schemes, Examples, and Computation Methods" IEEE Transactions on Industrial Electronics, 2019. 66(3): p. 1681-1692.

[18] Sami Rucho, "Modeling Demagnetization of Sintered NdFeB Magnet Material in Time-Discretized Finite Element Analysis", PhD. Thesis Aalto University, 2011, ISBN 978-952-60-4001-1.

[19] Juha Pyrh¨onen, Tapani Jokinen and Val´eria Hrabovcov´ "Design Of Rotating Electrical Machines", Second edition, 2014 John Wiley & Sons, Ltd.

Abbreviation and symbols

B	**Air gap flux density**	l_r	**Rotor length**
B_{max}	**Maximum air flux density**	m	**Mass flow rate**
B_r	**Magnet's residual induction**	R_{ph}	**phase winding resistance at working temperature**
B_t	**Total flux density of the magnet**	P_c	Stator copper loss
B_{rTref}	**Residual induction**	R_{ref}	**phase winding resistance at 20 °C**
C_M	**Torque coefficient**	T	**is the winding temperature**
c_p	**Specific heat of the coolant**	ΔT_{max}	**Maximum temperature difference between coolant and electric motor space**
D	**Inner diameter of the bearing**	T_{pm},	**PM thickness (mm)**
D_r	**Rotor diameter**	W_{pm}	**PM Width (mm)**
F	**Farmonic component frequency**	α	**Temperature coefficient of copper**
F_b	**Bearing load**	Ω	**Angular frequency of the shaft**
H	**Demagnetizing field strength,**	σ	**Electric conductivity of the magnet material**
H_{cJ}	**Magnet's intrinsic coercivity**	μ	**the friction coefficient**
i_{ph}	**Stator current / phase**	μ_0	**Permeability of free space.**
k_e	**Material-dependent coefficients of eddy current loss**	μ_r	**Magnet's relative permeability = 1.05**
k_h	**Material-dependent coefficients of hysteresis loss**	ρ	**Air density**
L_{pm}	**PM length (mm)**		